This paper is from conference:
SERI Second Wind Energy Innovative Systems Conference, volume II : December 3-5, 1980, :Broadmoor, Colorado Springs, Colorado / sponsored by U.S. Department of Energy; coordinated by Solar Energy Research Institute.

VARIOUS SYSTEMS FOR THE GENERATION OF ELECTRICITY USING UPPER ATMOSPHERIC WINDS

Bryan W. Roberts and John Blackler
Department of Mechanical Engineering
University of Sydney,
Sydney, N.S.W., 2006,
Australia

ABSTRACT

The strength and persistence of tropospheric winds generally increases with increasing altitude. In mid-latitudes the jet streams boost the available power densities to around 20 kW/m^2.

Six different tethered systems are reviewed. These range from balloons through fixed wing systems with open or ducted turbines. However, none of these systems are as attractive as a rotary-wing device, which is described in some detail.

Gessow's rotary-wing theory has been extended to justify a successful series of wind-tunnel tests on a twin rotor, gyromill. This machine can operate as a helicopter, generate in an auto-rotative mode, or manoeuvre in any of these modes. Transition from one mode to another is demonstrated.

A stability theory will be presented to indicate the ideal location of the tether attachment point or points, taking due account of the electrical conductors. A brief feasibility study is also given.

VARIOUS SYSTEMS FOR THE GENERATION OF ELECTRICITY USING UPPER ATMOSPHERIC WINDS

Bryan W. Roberts* and John Blackler**
Department of Mechanical Engineering
University of Sydney
Australia

1. Introduction

It has been suggested that it might be feasible to generate electricity using upper atmospheric winds. Particular reference has been made to jet stream winds. The main advantage in such a proposal is that as the operating altitude increases there is a resulting increase in the strength and persistence of the wind. The ultimate prize or maximum power availability occurs near the tropopause in mid-latitudes both north and south. In Australia the average power density at jet stream altitudes above a fixed site is of the order 16 to 18 kW/m^2. The isopleths of the average power density over the Australian continent are shown in Figure 1.

It can be seen that the average power density of this renewable energy resource is highly concentrated[1] when compared to other renewable, natural resources. On the other hand, this high power density is only attainable if one is prepared to accept the complication of an aerodynamic platform located in the tropopause at around the 250mb level.

This note is not intended to specifically relate to operations at the tropopause level. It acknowledges that the ultimate objective might be to obtain energy conversion at this level, but it also asserts that the strength of the tropospheric winds tend to increase favourably with increasing altitude.

Therefore, the concept of an aerodynamic or other platform located somewhere in the earth's troposphere would seem to have considerable merit from an energy conversion point of view.

Next, it is relevant to realise that the mechanical generation of electricity from winds at these altitudes invariably implies that certain aerodynamic drag loads will be produced. More specifically

---

*Associate Professor in Mechanical Engineering
**Design Engineer and Consultant, also Part-Time Lecturer in Mechanical Engineering

this means that the conversion of kinetic energy into electrical energy produces a drag force which is colinear with the free stream velocity vector. This drag force must be reacted if useful electrical energy is to be produced. In fact it is axiomatic in this paper (although not necessarily always so) that the drag load will be resisted by a tethering cable or cables. If these cables are to reach upwards through a significant section of the troposphere then they will need to be fabricated from high strength to weight ratio materials. Furthermore, it will be assumed that the uppermost end of the cable will be attached to the aerodynamic platform, and that no branch cables will be attached to this simple electro-mechanical cable. At the lower end the cable or cables will be wound onto a drum or drums, which may or may not be mobile across the earth's surface.

If we were to accept the above tethering concept to be applied at some convenient altitude in the troposphere, then the question arises as to what will be the preferred engineering configuration for the aerodynamic platform? In other words what should the platform look like, what devices should it carry in order to convert energy from the kinetic to the electrical form?

The current authors have to date investigated about six different configurations all of which have different advantages and disadvantages. There is, as a result, a whole series of hybrid systems which might be a composite of two or more of the basic concepts. These hybrids will not be discussed here.

The first object of this paper is to short list four different concepts and then to discuss the relative merits of each of these configurations. As part of a formal design process, it is strongly held that the advantages, disadvantages and technical feasibility of the short listed concepts must be appreciated prior to "working up" the most promising scheme.

2. Four Basic Concepts in the Design of a Tethered Aerodynamic Platform

Four different concepts will now be introduced, and they will be introduced in roughly chronological order. This chronological order refers to when the basic technology was first introduced commercially. This practice is useful in that the date of the initial commercial exploitation of any one system can be a rough guide as to the technical complexity of that concept.

2.1 The Airship Concept - Circa 1910

This broad concept is shown in Figure 2. A configuration might consist of a dirigible device to which is attached a number of propeller or other type wind turbines. The turbines could conceivably be located near the maximum cross section of the airship so that the velocity of the flow approaching the turbines is enhanced due to blockage effects. Fin and tailplane assemblies would be provided at the rear to achieve directional and longitudinal control.

Next it might be envisaged that the buoyant lift at the operating altitude will be slightly in excess of the all-up weight of the platform and cable system. Thus the device could remain aloft for extended

periods, regardless of the wind intensity at that altitude. In other words, the system would have no inherent stall phenomenon.

At full generating capacity, the drag due to power will be a dominant effect. This large drag, in combination with a much increased lift force, would be reacted by the tethering sub-system. This means that the platform's lift during peak power production must increase some three or four fold above the buoyant lift term. This extra lift could be achieved by tailplane action to nose-up the airship into a crude lifting surface altitude. This manoeuver would generate the extra dynamic lift.

As a result of the above manoeuver it is essential that the airship be clad with a substantial external skin in order to withstand the large dynamic pressures generated during the dynamic lift phase.

Finally, the expense of helium makes such a system unattractive as hydrogen is incompatible with the high lightning risk associated with extreme altitudes. However, the one big advantage of the airship concept is its ability to stay aloft for long periods regardless of the wind intensity.

2.2 The Open-Rotor Type Turbine and Biplane Concept - Circa 1930

This concept is shown in Figure 3, and it employs (along with the concept in section 2.4) a fixed wing system for the generation of lift. Again it must be appreciated that large dynamic lift forces must be generated so that a tethering cable can be used to react the drag loads associated with the production of useful electrical energy.

In this concept it might be argued that if a fixed-wing system is to be used, then a biplane, or multi-foil system, should give a lesser structural weight than a monoplane. On the other hand, there is a drag and aerodynamic interference penalty in the use of multi-foils, but this could be far outweighed by the superior structural performance of the multi-foil system.

Furthermore, it is envisaged that the turbines would have articulated blades in order to alleviate the large gyroscopic moments that will be associated with any turbine disk in the turbulent regions of the tropopause.[2,3]

Next it is most important to appreciate that there is one major, inherent disadvantage in the use of any fixed wing platform. This applies equally to monoplanes or multi-foils. This disadvantage relates to the necessity to have adequate winds aloft in order to avoid a system stall at the operational altitude. In other words, all fixed wing devices will have an inherent stalling speed.

Extensive studies of the occurrence of calm periods have been made in reference (1). A brief summary of the calm wind occurrences over a typical one-year period is given below in tabular form. The fixed site chosen is Forrest (30°51'S, 128°06'E) in Western Australia, which is a good Australian site from an upper atmospheric wind point of view.

Calm Wind Summary
Forrest at 35,000 ft

Stall wind speed in knots TAS	20	40	60
Number of occurrences per annum below stall	26	72	86
On each occurrence the average period below stall - hours	9	21	33
Total hours per annum below stall	234	1512	2838
Percentage time below stall	2.7	17.2	32.4

It may be seen that the ability of a fixed wing aircraft to stay airborne without elaborate manoeuvers might imply a minimum wind speed of say 40 knots TAS at this altitude. At ground level air densities this stalling speed will be only 22 knots EAS. This low ground stalling speed implies that the machine by necessity will be light weight, large and rather fragile by modern standards. Furthermore, it is important to appreciate that the above stalling condition will occur some 70 times per year on the average. That is, at least on a weekly basis. To avoid the platform descending during these spells, which last for some 20 hours on the average, it will be necessary to: (a) land the platform; (b) maintain altitude by supplying electrical power from the ground while continuously tacking back and forth across the on-coming light winds; (c) employ some other novel feature. Any of these procedures seem to be difficult, certainly on a weekly basis. The first procedure (a) involving landing and taking-off again will be difficult due to the machine's fragility and sheer size. The only other approach to be seriously considered involves procedure (b). This is unattractive from an electrical feasibility viewpoint,[4] where in order to avoid undue electrical insulation weight in the tethering cable it may be necessary to employ a number (possibly twin) of bare, air insulated cables. To tack back and forth over some distance for 20 hours, on the average, trailing bare cables at about 45 kW potential difference would seem to the current authors to be a rather hazardous procedure. Furthermore, any fixed wing system will require large areas for landing, take-off and other associated management functions.

2.3 Rotary Wing Concept with Tail Rotor or Tailplane - Circa 1950

The current authors have considered a rotary wing system (gyromill) in some detail. The concept is shown schematically in Figures 4 and 5. In Figure 4 two, or even more, main rotors are located in a simple airframe in contra-rotation. A tail rotor, or tailplane with or without fin, can be used for pitch control. This rotary wing machine can operate as a helicopter in one of its modes or as an auto-rotative device, namely a braked auto-gyro, in another mode.

Now five different modes of operation of this machine are envisaged, and these will be discussed in conjunction with Figure 5.

(i) Turbine Mode - High Winds

At relatively high wind conditions, near the rated speed of the unit, the device will produce its rated electrical output. For this mode of

operation the tail unit will be used to maintain a shallow disk incidence to the on-coming flow. Adequate rotor thrust will be developed as the rotors are used to drive electrical generators mounted under each rotor via separate gearboxes. A typical rated speed might be about 90 knots, and the sizes shown in Figure 4 are our very first estimates[5] for a 1 Mw mean output system. Each rotor might have 4 or 6 blades depending on the more detailed analysis of the form that is to follow.

(ii) Turbine Mode - Light Winds

The auto-rotative power generation concept can be maintained down to below 40 knots although the kinetic energy in the wind is greatly reduced. At these lighter wind conditions a greater face of the rotors can be presented to the on-coming flow as shown in the second sketch of Figure 5. At these increased disk incidences, and with appropriate collective pitch control, it is possible to develop adequate thrust to remain aloft while still generating a significant electrical output. This aspect will be demonstrated below. As winds become lighter still the system no longer generates power but stays aloft using the well proven auto-gyro principle.

(iii) Hover Mode - Calm Winds

When the wind speed drops below the auto-rotative speed for a given system weight, then the rotors can be put into a hover mode. In this state the rotors can be powered from the ground electrical grid system in order to keep the machine aloft. This represents the true helicopter mode with the appropriate collective pitch settings being applied.

Extended hovering is not envisaged. The preferred procedure during long calm periods aloft would be to allow the system to descend and land.

(iv) Landing and Take-Off Mode

The system could be landed on a helipad type surface midway between the twin cables.[4] It is envisaged that the device could descend or ascend from an operating altitude in about 30 minutes. Therefore, the preferred operational sequence is for the device to return to the ground station on a more or less weekly basis (apart from any emergency situation) for ground checks and maintenance during these relatively calm spells aloft. In other words, the calm spells are now used to advantage when compared to the strategy given in the fixed-wing system (2.2 above). In short, *the occurrence of calm spells can be easily used to advantage provided the landing and take-off procedures are easy to execute.* The landing procedure will also save "pump-back" energy expended during a hovering sequence. The landing sequence could also be useful in an impending lightning situation.

(v) Emergency Alighting Mode

The platform should incorporate an emergency system whereby the rotors and their bearings may be isolated from the gearbox and generator sub-systems. Any on-board emergency would then produce "free running" rotors of suitable collective pitch setting so that these rotors can work against the winches during the emergency "haul-in" procedure. Velocities of 1000 to 2000 feet per minute might be envisaged.

In summary it has been shown that the rotary wing concept has a whole host of advantages because it integrates the generating and lifting functions into one element. The likely weight of this type of platform will be about one third the weight of an equivalent fixed wing system.

2.4 Ducted Turbines with Monoplane or Biplane Concept - Circa 1980

The ducted, or diffuser augmented, turbine concept has been extensively reported previously.[6] Therein an even number of turbines are either "buried in" an airframe or "podded" onto a convenient fixed wing device.

This concept, as with all fixed wing concepts, suffers from all the aerial management problems detailed in section 2.2 above. The advantage of a ducted turbine system relative to an open rotor system is that the power coefficient based on the disk area is greater in favour of the ducted system. However, an articulated, open rotor system has a greater power to weight ratio than the ducted system. In addition, the ducted system, with or without segmented sections, is inherently sensitive to duct separation problems particularly under yaw or pitch incidences. The latter incidence is likely to be critical in the highly turbulent conditions in the region of the tropopause.[3] It is not intended to discuss this concept at length here, as it has already been the subject of a number of papers.

2.5 Some General Comments

A number of different concepts have been examined. The discussion has highlighted the aerial management problems associated with fixed wing systems, along with the inability of the airship to achieve extreme altitudes while withstanding high wind velocities.

The authors wish to go on record that the rotary wing concept appears to be the only pragmatic solution to the tethered, upper atmospheric windmill system. However, other workers may be able to evolve other practical, alternative proposals. In the current paper we will now examine concept 2.3 above in some detail.

3. Experiments with a Rotor Test Vehicle

In order to examine the auto-rotative generation principle it was decided to construct a simple, flap-articulated rotor system above a test vehicle. By moving the test vehicle through still air one could obtain a confirmation of the auto-rotative principle along with an estimate of the accuracy of the theoretical predictions.

In the trunk of a car a tower was added in the form of a space framed structure. To this was added a rotor shaft, a step-up gearbox and a separately excited DC machine. These latter three elements were capable of being locked at any control axis angle, α, by rotating them in trunnion bearings. The DC machine was arranged to form a swinging dynamometer in order to measure directly the torque produced by the rotor. The assembly is shown in Figure 6 where α is in the range $0° < \alpha < 60°$.

The rotor blades themselves were constructed from fibreglass bonded in epoxy resin. The blade twist was linear at $+8°$, while the collective pitch angle was pre-set using specially machined blade grips. A

collective pitch setting of -8° has been used in tests to date. In addition, the two blades featured individual flapping hinges with a 4" offset without drag articulation. The rotor has a tip radius of 4.15 feet with a solidity of 0.06. The blades were of an NACA 0012 section with a 5.25" chord.

For any particular control axis angle, the speed of the rotor is governed simply by the vehicle speed and the degree of external excitation on the DC generator. The rotor was designed for speeds up to 1500 rpm.

It was decided to measure only the rotor torque at this time, and not bother measuring the thrust. If the $2C_Q/\sigma$ coefficient could be shown to agree with the extended Gessow theory, then it was highly likely that the thrust coefficient would agree, since both resulted from a common theory.

A proportional feedback was used to control the separately excited field in order to maintain a pre-set rotor rpm. A manual over-ride allowed a field rheostat to be used to control rpm if the manual mode was ever required. Data was collected during the months of November and December 1979, and typical results are shown in Figure 7. Therein $2C_Q/\sigma$ is a function of μ for α fixed at a value of 29.2°. Furthermore, the notation used from hereon is standard and defined in reference (7).

The results shown in Figure 7 are encouraging. The $2C_Q/\sigma$ values are somewhat less than the calculated values using the accepted section profile drag values. However, they agree well when allowance is made for increased drag at the model Reynolds number. The conventional method of allowing for increased profile drag due to retreating blade stall is also substantiated by the test results. A general roughness in the test vehicle in the stall region is further evidence of this effect.

Generally, we were most encouraged with the test vehicle's performance. In fact, it was immediately decided to build a flying model into which would be installed an auto-rotative generating system similar to that installed in the car. The construction and performance of this model is now described.

4. Flight Experiments with a Model Gyromill

It was decided to use a side by side twin rotor assembly with the rotors running in contra-rotation. In this arrangement the torque reaction moments in the helicopter, or power generation mode, would be balanced more or less. In order to avoid having gearboxes between the rotors and the motor/generator system it was decided to use rotors directly mounted on small high rpm motors/generators. These motors were permanent pole DC machines of robust construction found in cars, therein operating as electrically driven radiator fan motors. A pair of these motors were modified to save weight and the armatures bonded so that they could be run at up to 8000 rpm without dislodging the windings. One motor was modified in the brush region to allow for correct brush lag when that motor/generator was running in the reverse direction.

The motors were bench tested in the full motoring and generative modes by driving or having them driven using a DC source and an armature

control rheostat. Generally the system has worked well to date, although such a system is in no way proposed for any larger scale gyromill system.

The model is shown in Figure 8 mounted on twin "tethers". The main, twin pivots, represent attachment points of the airframe to the two tethers, and they may be seen on the motor frame just below the rotor heads. The tethers, in this instance, are represented by metal bars pivoted on a shaft mounted just below the tunnel floor. These shaft pivots are adjacent to the two floor slots. A light bracing of internal rods makes a tethering frame which effectively eliminates the yaw component.

The rotors were directly mounted on the motor shafts through a pair of flapping hinges at about a 3/4 inch radius. The rotor themselves were approximately 26-inch diameter with two untwisted blades of NACA 0012 section. The blade chord was 1¼ inch which gave an effective solidity of 4.88%. The in-board blade element was some 2-inch long, and this was simply a pair of flexible spring steel strips in order to achieve 12° of collective pitch movement. In this way small pitch bearings were eliminated. However, such a system is of limited life and is in no way proposed, or inferred, for larger versions.

The rotors featured only collective pitch control; cyclic pitch control has been completely eliminated. The pitch stability and control was provided by the all-moving tailplane.

The collective pitch of the rotors was controlled by a quite heavily loaded linkage and actuator system shown in-board of each motor/generator in Figure 8. This control is independent and remotely controlled by a manually actuated, standard radio control link.

The tailplane is all-moving and can be likewise controlled manually by the radio control system. The incidence of the tailplane can change through up to 90° in order to accommodate the extreme fuselage altitudes from pure hovering to the auto-rotative generate mode.

A balance weight is mounted on a forward string in order to give some adjustment to the longitudinal position of the C of G. This is a dominant term in the pitch stability equations.

A series of hover trials were initially performed on the basic airframe in May 1980 to check the rotor performance in the demanding hover situation. The original 12-volt motors were driven by a 48-volt source with a 19 amp current in order to check the motor system for short, hovering flights. It being realised of course that the hovering mode is the most demanding mode from a rotor power viewpoint. From a stability aspect the twin, contra-rotating rotor system was more than satisfactory.

The gyromill was then test flown in the University's 7 × 5 foot low speed wind tunnel during July 1980. The system in auto-rotative generating flight is shown in Figure 9, where the free stream flow is from right to left. In this photograph the attachment of the tethers to the airframe is at a pair of pivots shown just forward and below the centre of the airframe's main cross-tube.

In summary the model gyromill can pitch relative to the tethers on the airframe-tether pivots. It can climb and descend on the end of the rigid tethers since the tethers are free to rotate about pivots just below the tunnel floor. Extensions to the tether bars below the tunnel floor allows balance weights to be added to the tethers. In this manner it is possible to vary the effective weight of the machine relatively to the rotor thrust. It will be shown that the parameter, w, is important in determining the flight envelope, where w is defined as

$$w = \left(\frac{2W_p}{\sigma a}\right) \Big/ \left(\frac{2C_T}{\sigma a}\right) \pi R^2 \rho (\Omega R)^2 \qquad (1)$$

and W_p the weight of the complete gyromill platform.

The machine has performed very well to date. We have been able to climb and descend in the helicopter mode with the system shown in Figure 8, except that the airframe-tether pivots have been moved to a somewhat more favourable location to improve the pitch stability. The machine has then been converted from the full helicopter mode to the auto-rotative power generation mode as the tunnel speed has been increased from zero wind speed to some 45 ft/sec. The reverse procedure can also be achieved.

During the conversion from helicopter to auto-rotative power generation the blade collective pitch has been varied from about +10° to +2° on both rotors simultaneously. The matching tailplane incidence is also varied during this manoeuver in order to maintain the correct airframe, or disk incidence, relative to the free stream. At all times the system was stable and easily controllable from the manually controlled radio link. Power inputs, and then outputs when in the generate mode, were likewise controlled manually with a pair of rheostat sliders.

It was also very easy to achieve a fully auto-gyro type take-off and landing at large disk incidences. In these manoeuvers the rotors were spun-up with the airframe grounded in a nose-up altitude of some 20°. As the wind increased full auto-rotation was achieved by collective pitch control, and then the device was flown off by inducing the lift-off incidence through tailplane action. The reverse procedure for landing was also obtainable.

The preliminary testing and the data reduction is now complete, and some of the results are reported herein as Figures 10, 11 and 12. Figure 10 shows a comparison between the measured torque coefficient and the extended rotor theory for $\theta_0 = +2°$, $\theta_1 = 0°$. All results given here apply to this collective pitch angle and to values of μ in range $0.1 < \mu < 0.15$. No blockage nor tunnel corrections have been applied, since, it is argued, the results here only serve to indicate that the system is generally predicable. The Reynolds number involved are about one order of magnitude removed from a realistic, practical system and no corrections have been made to profile drag etc., to allow for this significant effect. Therefore, we might conclude that the extended rotor theories that are currently available are entirely adequate for a more detailed future analysis of the gyromill system. Figure 10 also shows the control axis angle, α, as a function λ for two values of μ. The experimental points here relate to experimental μ values for cases $.095 < \mu < .105$ and $.145 < \mu < .155$.

Figure 11 shows a comparison between the experimental thrust coefficients and the extended theory. Again no tunnel corrections have been applied to the data for the same reasons given above.

Finally, Figure 12 gives the tailplane effectiveness in achieving longitudinal control. The figure shows the steady tail incidence angle that is necessary to maintain a certain airframe incidence when the rotor thrust is at the value given on the abscissa. This graph only applies to a wind speed of 46.5 ft/sec, and the curve drawn is the mean of the experimental results. Of course, the slope of this curve will vary with the location of the C of G and the airframe-tether pivot axis. Furthermore, the tail volume coefficient on this machine is 0.22, the precise definition of which is given in the upper right hand corner of the figure.

One can conclude this section with the categoric statement that the configuration seems to be statically stable, it is manoeuverable and generally complies with rotorcraft theory. Above all we are confident that the mode conversions from the helicopter state to the auto-rotative power generation state, and vice versa, can be achieved easily and pragmatically.

5. The Aerodynamic Efficiency of a Generating Rotor

The aerodynamic efficiency, η, of a generating rotor can be simply defined as the power produced at the rotor shaft relative to the power available in a cylinder of on-coming wind. The diameter of the cylinder is equal to the rotor diameter.

The rotor diameter is used as the reference area regardless of the disk inclination, and this reference is in agreement with Glauert's original and accepted assumption in helicopter theory. Therefore, the aerodynamic efficiency may be defined as

$$\eta = C_P \rho\pi R^2 (\Omega R)^3 / \tfrac{1}{2}\rho v^3 \pi R^2 \qquad (2)$$

where the symbols are as defined in reference (7). Next it is noted that

$$C_P = C_Q \qquad (3)$$

and

$$\mu = V \cos\alpha / \Omega R \qquad (4)$$

so that the expression (2) for efficiency can be written as

$$\eta = 2C_Q (\cos\alpha/\mu)^3 \qquad (5)$$

Now in the case of an ideal rotor, where the blades are assumed to have zero profile drag and no other power losses exist, then it can be shown that the ideal aerodynamic efficiency, η_I, is

$$\eta_I = 2C_T \lambda (\cos\alpha/\mu)^3 \text{*} \qquad (6)$$

Special cases of equations (5) and (6) apply when $\alpha = 90$ and $\mu = 0$. This corresponds to the conventional windmill configuration when the disk is normal to the free stream. In this case equations (5) and (6) reduce to equations (7) and (8) respectively.

*For simplicity the resultant force is assumed parallel to the control axis.

$$\eta_{\alpha=90} = 2C_Q\left(1/\lambda + C_T/2\lambda\right)^3 \tag{7}$$

and

$$\eta_{I_{\alpha=90}} = 16/27 = 59.3\% \tag{8}$$

where the latter equation agrees with the well known Betz-Lanchester efficiency for a conventional windmill.[8] Further algebraic work on equation (6) yields the result that the ideal efficiency at any particular α value will be at a maximum at a certain (λ/μ) value. In mathematical form we may write that

$$\eta_{I_{max}} = 4\{(\mu/\lambda)^2 + 2\}^2/[(\mu/\lambda)^4 + 7(\mu/\lambda)^2 + 9] \tag{9}$$

where

$$\alpha = \tan^{-1}[\lambda/\mu\{2(\mu/\lambda)^2 + 3\}/\{(\mu/\lambda)^2 + 2\}] \tag{10}$$

Equations (9) and (10) are plotted on Figure 13. Therein it may be seen that at all values of α the ideal aerodynamic efficiency is always less than the Betz efficiency. Furthermore, at any particular α value the efficiency given by equation (5) will always be less than the corresponding ideal efficiency value.

This ideal efficiency cannot be achieved in practice due to two main effects. In the first instance a portion of the power extracted from the wind is required to overcome the blade profile drag. This gives a reduced aerodynamic efficiency at any α value depending upon the blade characteristics. In the second place, this reduced efficiency is not always achievable due to the possibility of rotor blade stall on the retreating side of the rotor disk. Both these effects have been observed in the experiments reported in section 3 above on the rotor test vehicle.

The Gessow extended theory will now be used to predict the limits beyond which the second effect renders the rotor operation unacceptable. In this calculation we will use a standard NACA 0012 section with the accepted profile drag values as given in reference (7). In this case equation (5) is simply

$$\eta = \eta(\sigma, \mu, \lambda) \tag{11}$$

When the Lock number is 4.7, the tip loss coefficient is 0.95, $\theta_0 = +2^\circ$ and $\theta_1 = 0$ then the plots of aerodynamic efficiency are given in Figures 14 and 15 for solidities of 0.05 and 0.10 respectively. Therein the incidence reference limit has been drawn at $\alpha_r(1.0, 270) = 15^\circ$. In Figure 14 when $\mu = 0$ it can be seen that $\eta = 0.50$ at this value of α_r. Here the aerodynamic efficiency curve has been terminated in a dark circle. Operation beyond this point (i.e. to the right of the dark circle) is not possible because of blade stall effects. For increasing values of μ the blade stall effects occur at lower values of the in-flow parameter, λ. Furthermore, it is worth pointing out that with a tip speed ratio, μ, of zero in helicopter terminology, the tip speed ratio, $(\Omega R/V)$, in windmill terminology is about 7.7 at the point where the aerodynamic efficiency reaches its local maximum value of 0.50.

Figure 15 shows the aerodynamic efficiency at a solidity of 0.10. Again the efficiencies are always less than the Betz value of 16/27. However, it is also interesting to note that at a tip speed ratio of 0.1 the efficiency is always greater than the efficiency associated with a tip speed ratio of zero.

The object of the discussion in this section of work is to indicate that classical helicopter theory can be extended to include articulated windmill theory. We have not seen this reported elsewhere. In addition it is possible to use well established values of $2C_Q/\sigma$ to define a realistic aerodynamic efficiency for the conversion of wind energy into shaft work. For all α values the practical Gessow theory gives an efficiency which is always below the Betz efficiency. Also the ideal aerodynamic efficiency defined herein is always greater than the practical aerodynamic efficiency defined by equation (5) above.

6. Characteristics of the Tethering System

In a previous publication[6] the mechanics of the tethering system was described. In particular, the strength to weight ratio of the tensile component of the cable was shown to be of prime importance. The effects of cross-wind, gravity and the conductor elements were all included. In this section these prior results will be reorganised to interface with the mechanics of the rotary wing platform.

As discussed in section 2 above, it will be assumed that the tethering system will consist of dual cables. When these tethers reach to high altitudes with resulting high electrical voltages, the insulating material will not be provided.[4] This constitutes a considerable weight saving as the dual conductors/tethers are then air insulated. For demonstration purposes, and not necessarily as a firm system proposal, we will examine a 1 Mw mean output gyromill which is tethered by dual cables each attached directly under the twin rotor axes. It will be assumed in the demonstration that the equivalent conductor area in each tether is 12 mm^2. The conductor is taken as an aluminium, multi-filament sheath around a kevlar core. The kevlar is further assumed to be bonded in a flexible resin matrix.

In addition, it will be assumed that 5% of the tensile load is carried by the aluminium and the remainder by the kevlar. This allows for the weaves and the relative elastic moduli of the materials involved. A further 15% will be arbitrarily added for dynamic effects and a general reserve factor of 1.5 will be applied. Finally, for the variation of cross-wind with altitude we will take the yearly average profile at Forrest, W.A., with a peak wind of 90 knots at the extreme altitude.

Under these assumptions the tethering system can reach to 35,000 ft. This altitude has been chosen for demonstration purposes. Such an altitude is not necessarily optimal, nor is it claimed to be practically achievable. It is only chosen in order to demonstrate the interfacing problems and how these might be solved in a pragmatic fashion. It is strongly held that the principles which follow must be appreciated technically, before any viable economic analysis is undertaken.

Figure 16 gives a summary of the cable characteristics. T_0 is the cable tension at the upper attachment point. W_c is the cable weight while θ is the slope of the cable relative to the horizontal at the uppermost end. Figure 16 summarises the issues in that (W_c/T_0) can be plotted as a function of θ for various levels of T_0 ranging from 4,000 to 10,000 lb. The conductor diameter is constant at 3.9 mm.

The latter sentence implies that as the scale of T_0 increases so the value of (W_c/T_0) should reduce slightly for a specific θ. This is because the weight of the fixed conductor represents a lesser proportion of the total weight as T_0 increases. In the figure the ratio (W_c/T_0) actually increases with the scale of T_0 for a fixed θ. This is due to the effect of the cross-wind. The cable becomes larger as T_0 increases and this introduces a greater influence than the influence due to the effective weight reduction associated with a fixed conductor size. These two effects are second order only. However, they are acknowledged but will be neglected in the calculation that follows. In other words, these second order effects should be included in a thorough optimisation study, but they do not add to the practical discussion given below.

Therefore, we will assume that (W_c/T_0) is independent of the scale of T_0 and the lower curve in Figure 16 will be assumed for further demonstration. The approximate structural limit in Figure 16 occurs when (W_c/T_0) is about 0.34. This value gives the maximum value of θ that this particular kevlar-aluminium cable may drape without rupturing.

7. Interfacing a Twin Rotor Gyromill with a Dual Cable Tethering System

The following analysis will now interface the cable system described above onto a typical gyromill platform. Again second order effects will be neglected, but they will be acknowledged as they occur.

We will proceed by assuming that the gyromill is a symmetric, twin rotor assembly featuring appropriately twisted blades. Let the twist, θ_1, be $+8^\circ$ which is a reasonable choice for an auto-rotative system. Use an NACA 0012 blade section, and let the collective pitch angle, θ_0, lie in the range 0° to -12°. The solidity of the rotor at this stage will be left open.

Next derive from the extended Gessow theory the torque and thrust coefficients for the rotors described above. The case of $\theta_0 = -8^\circ$ is shown in Figure 17, and similar curves and have been found for the above collective pitch range. The tip speed range of interest lies from 0.05 to 0.25. In the figure the torque and thrust coefficients are plotted as functions of λ, the in-flow parameter. The incidence reference angle, α_r, refers to the normally accepted blade incidence at a U_T of 1.0 and a ψ value of 270° in standard notation. This means practically that retreating blade stall effects will become important when $\alpha_r > 12^\circ$. We will be somewhat optimistic and work with a maximum value of α_r of 15°. Modern blade sections might be able to achieve this value. An interested reader may choose any other value without detracting from the discussion that is to follow.

The next step is to decide on a logical procedure for integrating the tethering cables into the gyromill system in a reasonably optimal fashion. One might argue that the optimal arrangement is one in which

the return on capital investment is at a maximum. Another optimising criterion might be one in which the system maximises the overall conversion efficiency, or another which maximises the generating factor (see below) of the total system. Alternatively, an optimal arrangement might be one in which capital cost per unit of installed capacity is at a minimum, or one which minimises the cost of the energy so produced. Finally, the optimal arrangement might be chosen to save the maximum amount of liquid fuel if these devices were used in a diesel powered grid network so common in outback Australia.

The current authors accept all these notions, and they expect that the final optimisation, against certain favoured criteria, will be ultimately the choice of electrical network engineers. In the meantime some headway can be made by introducing the notion that a near optimal arrangement will be one which maximises the ratio of the power output to the total system weight, while producing a high generating factor. This implies that the system will be capable of producing a useful power output at a very low wind speed.

One might, therefore, argue that the power to platform weight ratio will be some certain optimal value, and to this value must be added the minimum cable weight system in order to strike the most promising overall power to weight ratio for the whole system. In mathematical form, the optimal power to total weight ratio is achieved when f is at a maximum.

$$f = \left(\frac{2C_Q}{\sigma} \Big/ \frac{2C_T}{\sigma a}\right)\left(\frac{T_0}{W_c}\right) \Omega R \qquad (12)$$

It is reasonable to assume that ΩR is not a significant variable since in any practical rotor it will be chosen at a high value consistent with minimum compressibility effects. Thus ΩR is deleted. It can be shown that equation (12) is simply

$$f = f(\lambda, \mu, \sigma) \qquad (13)$$

where the form of f is shown in figure 18 for the case $\sigma = 0.10$. Similar curves have been found for $\sigma = 0.05$ and 0.20. In constructing these curves it is necessary to realise that the (T_0/W_c) value found in Figure 16 depends on the two following auxiliary equations with the assumption that the platform weight to total tether tension force is zero.* This is a second order effect.

$$\alpha = \tan^{-1}\left[\lambda/\mu + \frac{C_T}{2\mu(\mu^2 + \lambda^2)^{\frac{1}{2}}}\right] \qquad (14)$$

and

$$\theta = [90 - (\alpha + a_1)] \qquad (15)$$

where a_1 is the first harmonic, longitudinal flapping angle.

Each of the curves for a fixed solidity, see Figure 18 for instance, give f as a rising curve when read from left to right with θ_0 and μ held constant. The f curves are extended to the point $\alpha_r = 15°$, where a dark

*In actual practice this ratio will be about 0.15 instead of zero. See below for further discussion.

circle has been inserted. The loci of maximum f is simply a curve joining the dark circles when $\mu = 0.2$. The maxima values of f are to be found slightly to the left of the dark circles when $\mu = 0.1$.

In all cases the relevant maxima curves indicate that the power to cable weight ratio improves with increasing μ. Close examination of the curves for $\sigma = 0.05$, 0.10 and 0.20 indicates that σ is a very soft parameter in this range. Therefore, a mid-range choice of $\sigma = 0.10$ might be suitable for our purposes. This choice is shown in Figure 18.

Having chosen the solidity it now remains to select the relevant conditions corresponding to a high value of f in Figure 18. On one hand the magnitude of f improves with increasing μ. On the other hand, at high values of μ the value of V, the free stream velocity, will tend to be excessive for a compressibility limited maximum rotor tip speed. High values of V in turn imply poor generating factors. Therefore, on balance we will choose the following conditions for operation at a maximum power output to cable weight ratio: $\theta_0 = -12°$; $\theta_1 = +8°$; $\lambda = 0.154$; $\mu = 0.20$; $\sigma = 0.10$. *Furthermore, it is important to note that this local maximum occurs at the maximum possible value of* α_r, *namely 15°.*

In concluding this section of the work, we have now effectively specified the rated or peak condition of the system by choosing the above set of parameters. While the weight of the platform itself has been neglected at this stage it will be included in the next section. One is simply stating that a local optimisation of the power to cable weight ratio should be a rough guide to the low wind performance of the system at altitude.

8. The Complete Operational Envelope for a Gyromill

Having selected the values for θ_0, θ_1, λ, μ and σ given above, it is now possible to construct the complete operational envelope for the complete gyromill assembly.

Proceed by again assuming that the ratio of the platform weight relative to the total tether tension is negligibly small. Other values of this ratio will be discussed in just a moment, but the zero ratio case is the easiest situation to logically describe initially.

Therefore, Figures 16 and 17 along with equations (14) and (15) can be used to construct the gyromill operational envelope shown in Figure 19. The ordinate shows the function $(\alpha + a_1)$ which is physically the incidence of the rotor tip path plane. It should be realised that the normal to this tip path plane is the approximate direction of rotor thrust vector (see Gessow[7] p. 183). For a given α and θ_1 it is possible to plot $(\alpha + a_1)$ against λ for various values of θ_0 and μ. This has been completed in Figure 8 for the range of variables $-12° < \theta_0 < 0°$; $0.07 < \mu < 0.25$.

Lines of constant values of θ_0 and μ are shown as curves rising from left to right. It will be noticed that each curve is terminated, in general, in a black circle. This symbol represents the $\alpha_r = 15°$ position, similar to the symbols used in Figures 14, 15 and 17. Furthermore, it should be noted that the faint, near-vertical lines

join points of equal θ_0 at the condition $\alpha_r = 15°$. These vertical lines represent the physical limit to the rotor operation at the appropriate values of θ_0 and μ.

Next, if we assume that the platform weight to cable total tension ratio is negligible, then it should be realised that the structural limit ($\theta = 29°$) given in Figure 16, in conjunction with equation (15), implies the maximum possible tip path incidence is

$$(\alpha + a_1) = (90 - \theta_{min}) = 61°$$

for the kevlar-aluminium system operating to an altitude of 35,000 feet given above. In other words, when the weight of the platform is negligibly small, the maximum tip path incidence is 61°, and this represents the $(\alpha + a_1)_{NE}$ value. Therefore, we can draw the uppermost horizontal line on Figure 19 through the ordinate value of 61°. Label this line as $w = 0$

where
$$w \equiv \frac{\left(\frac{2W_p}{\sigma a}\right)}{\pi R^2 \cdot \rho (\Omega R)^2} \Big/ \left(\frac{2C_T}{\sigma a}\right) \qquad (16)$$

and W_p is the platform weight.

Now we shall investigate non-zero values for W_p. In the general case, when w is small, it is a simple matter to show that the rotor thrust line and the cable tension vector are very nearly equal and separated by a small angle β, where β is given by the expression

$$\beta \simeq 57.3\ w \sin(\alpha + a_1) \qquad (17)$$

Therefore, for small values of w, the maximum achievable values of $(\alpha + a_1)$ are given by the horizontal lines labelled with the appropriate value of w. It is worthwhile pointing out that a likely practical value of w is between 0.15 and 0.20 for a large scale machine. Of course, this value of w will be a function of the operational altitude here taken as 35,000 feet for demonstration purposes only. For practical machines at lesser altitudes the value of w may tend to be less than the abovementioned figures.

The complete operational envelope is now contained in Figure 19. The appropriate upper horizontal lines give the $(\alpha + a_1)_{NE}$ values for a range of the w parameter. The gyromill can be operated along the horizontal line provided the cable tension does not exceed the design value.

The right hand bound to the flight envelope is limited by the minimum collective pitch angle that can be obtained by the rotor head, or by maximum power to cable weight requirement given by the point $\theta_0 = -12°$; $\theta_1 = +8°$; $\mu = 0.20$; $\sigma = 0.10$.

At this optimal power to cable weight ratio, the cable is in its most favourable configuration. This point is denoted as point A in Figure 19. For a reducing wind speed the preferred strategy is to move along the $\alpha_r = 15°$ locus to point B, while *maintaining* the cable tension at the maximum design value. This will ensure the maximum power output. From

point B the strategy is to operate along a horizontal line (here chosen as w = 0 for convenience) through points C, D and E until the wind speed is insufficient to maintain altitude somewhere to the left of point E. Along the line AE the cable tension is again *maintained* at its maximum design value. In fact it is axiomatic that for maximum power output in any flight configuration α_r should be at its maximum (namely about 15°) and that the cable should be at maximum tension. These two conditions ensure the maximum power strategy. Operation anywhere inside the rectangle of Figure 19 is permissible.

A typical example will now be given to show the simplicity of the operating procedure, and above all to demonstrate use of the operational envelope given in Figure 19.

9. A Typical Design Study

Assume we wish to design a twin rotor gyromill whose mean power output is to be ½ Mw at each of the rotor shafts. Further assume that the device is to be operated at 35,000 feet in a standard NACA atmosphere above Forrest in Western Australia, where the annual velocity-duration is as shown in Figure 20.

From this velocity-duration curve it is useful to draw the annual power available duration curve for the same site. This latter power-duration curve is shown as Figure 21.

Next enter this study by designing a system to operate at the rated condition at point A of Figure 19. Assume w = 0 for simplicity and neglect any airframe forces and tailplane forces.

9.1 Design for Operation at Point A

From Figure 19 it follows that $\mu = 0.20$, $\lambda = 0.513$, $\theta_0 = -12°$, $\theta_1 = +8°$, $\sigma = 0.10$, $\alpha_r = 15°$, which gives $2C_Q/\sigma = 0.030$ and $2C_T/\sigma a = 0.0380$. The desired peak output to produce a mean output of ½ Mw per rotor is in fact 985 HP per rotor.* Furthermore, assume that the maximum tip speed of the rotor is 600 ft/sec, a more than comfortable value.

Under these conditions it follows immediately that

$D = 53\frac{1}{2}$ ft Disk area = 2248 ft ΩR_{max} = 600 ft/sec
$\sigma = 0.10$ bcD = 449.6 ft

At this condition it also follows that

$T_0 = 6556$ lb/side $(\alpha + a_1) = 41.3°$
$W_c = 918$ lb/side V = 94.2 kts (rated wind speed)

9.2 Design for Operation at Point B

From Figure 19 it follows that as more cable is run-out the cable tension remains constant at its maximum permissible value of 6556 lb. Thus $\mu = 0.103$, $\alpha_r = 15°$, $2C_T/\sigma a = 0.0395$, $2C_Q/\sigma = 0.0312$, $\lambda = 0.154$ and $\theta_0 = -12°$. Under these conditions it follows that

---

*This figure has been found from an iterative design process. Only the final iterative calculation has been shown herein.

$P = 985$ HP	$W_c = 2228$ lb/side	$V = 72.2$ kts
$T_0 = 6556$ lb/side	$(\alpha + a_1) = 61°$	$\Omega R = 592$ ft/sec

9.3 Design for Operation at Points C, D and E

The strategy is to operate along the w = constant horizontal line in Figure 19. The calculations for points C, D and E are exactly similar and we need only quote the results for point E.

Under conditions at point E no more extra cable is run-out compared to point B, but the system is again operated at the maximum permissible tension.

$P = 313$ HP	$W_c = 2228$ lb/side	$V = 41$ kts
$T_0 = 6556$ lb/side	$(\alpha + a_1) = 61°$	$\Omega R = 495$ ft/sec

The power output from the system can now be plotted onto a power output-duration curve using Figure 20 as a parametric function. In this case the annual power output-duration curve is shown as Figure 22.

In this figure the peak output is maintained from a peak wind speed of 94 kts down to a much lesser wind speed of about 72 kts. This surprising and encouraging result is simply due to an opening of the disk face to the on-coming wind by increasing $(\alpha + a_1)$ from 41° to 61° in going from point A to point B.

A low wind strategy is adopted from point B down to point E and beyond. Again the system is capable of producing 313 HP at only 41 kts wind speed due to a collective pitch change from -12° to 0°.

It is interesting to compare the mechanical efficiency and the tip speed values at each of these points. At no time does the tip speed exceed 600 ft/sec, while the mechanical efficiency varies from 14% at point A up to some 43% at point D. See Figure 22 for efficiency and speed details.

Finally, the single most important entity can be now derived from Figure 22. This is the generating factor and is used by electrical network engineers in grid planning. This factor is simply the ratio of the mean to peak power output. The system herein designed has a generating factor of 670/985, namely 68%. Furthermore, it is interesting to note that the available power-duration curve in Figure 21 has a generating factor of only 48%, if the conversion efficiency is held constant. However, due to the "lay-back" rotor effect, or the increase in $(\alpha + a_1)$ term, there results a dramatic improvement in the generating factor. In other words, the increased incidence effect can be used to enhance the generating factor by some 41%, namely from 48% to 68%.

Finally, it should be stressed that this design has been given to highlight the technical features inherent in any thorough study. The assumptions and altitudes used are introduced only for demonstration purposes and do not necessarily represent a final design.

10. Acknowledgement

We acknowledge the assistance of the Australian National Energy Research, Development and Demonstration Council in the work reported herein.

11. References

(1) J.D. Atkinson, C.A.J. Fletcher, J.L. Milthorpe and B.W. Roberts, "The Use of Australian Upper Wind Data in the Design of an Electrical Generating Platform", Charles Kolling Res. Lab. T.N. D-17, June 1979, University of Sydney

(2) U.S. Air Force "Handbook of Geophysics"

(3) "Atmospheric Turbulence and Its Relation to Aircraft", U.K. Ministry of Aviation Symposium, RAE Farnborough, Nov. 1961

(4) Merz and McLellan & Partners, "Transmission and On Board Electrical Plant" for University of Sydney, July 1979

(5) B.W. Roberts, "Various Engineering Concepts in the Design of an Aerodynamic Generating Platform", Charles Kolling Res. Lab. T.N. D-19, July 1979, University of Sydney

(6) C.A.J. Fletcher and B.W. Roberts, "Electricity Generation from Jet-Stream Winds", Journal of Energy, Vol. 3, No. 4, July-August 1979, pp. 241-9

(7) A. Gessow and G.C. Myers, "Aerodynamics of the Helicopter", Macmillan Co., N.Y., 1952

(8) K.H. Bergey, "The Lanchester-Betz Limit", Journal of Energy, Vol. 3, No. 6, Nov.-Dec. 1979, pp. 382-4

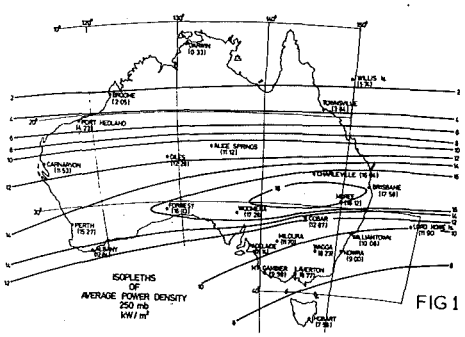

FIG 1

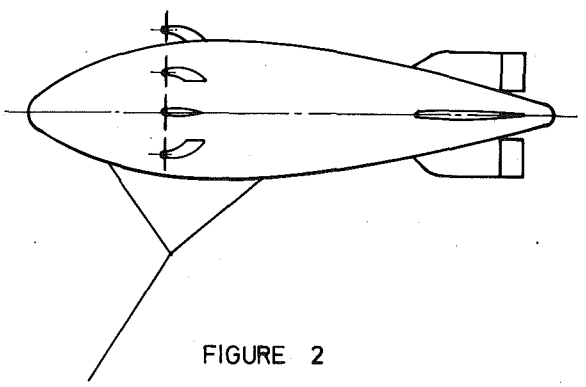

FIGURE 2

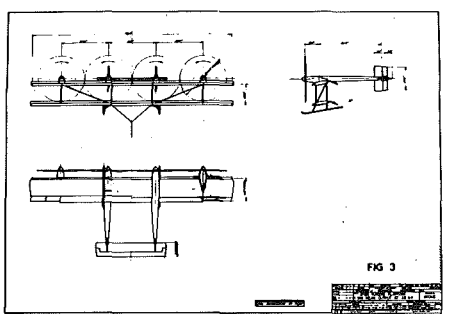

FIG 3

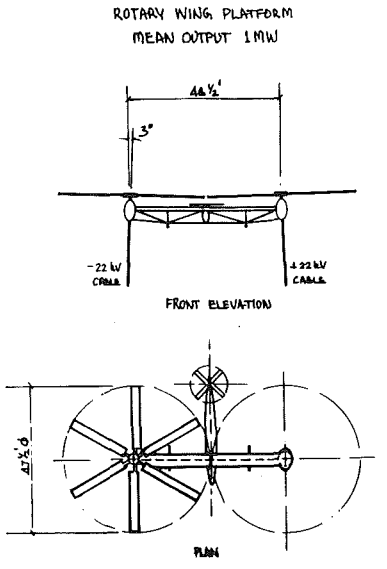

FIGURE 4

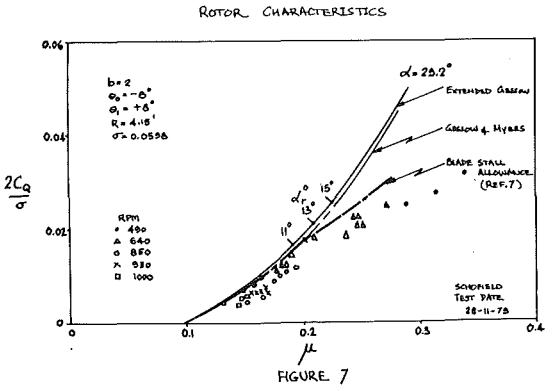

FIGURE 7

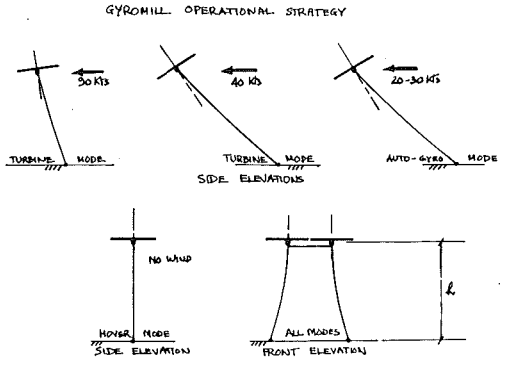

FIGURE 5

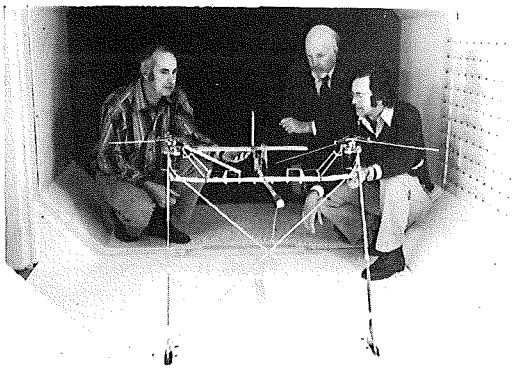

Figure 8

Figure 6

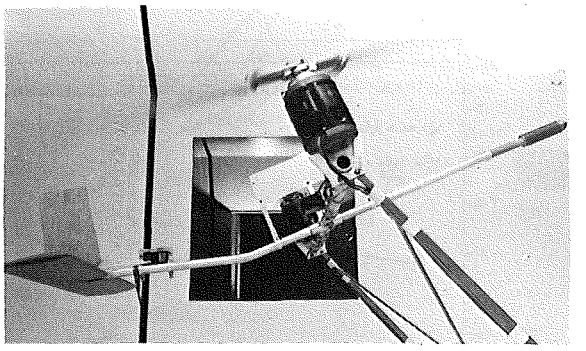

Figure 9

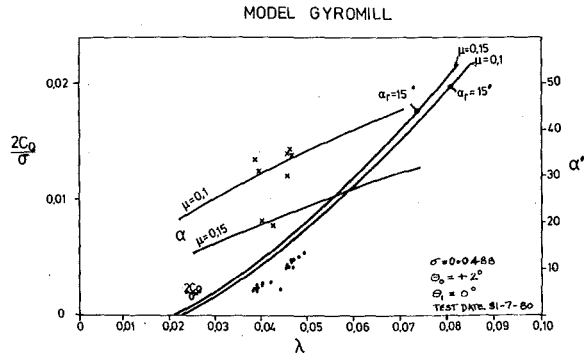

FIGURE 10

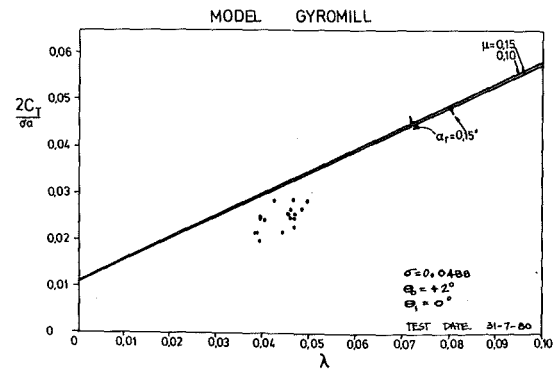

FIGURE 11

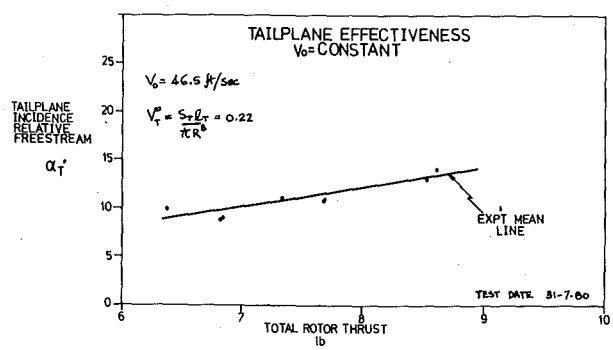

FIGURE 12

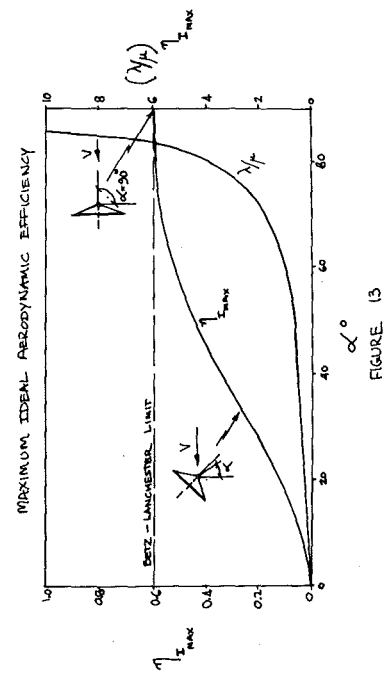

FIGURE 13

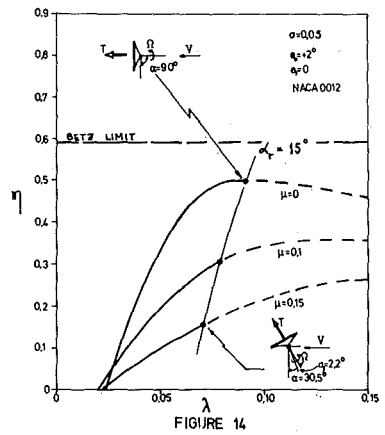

FIGURE 14

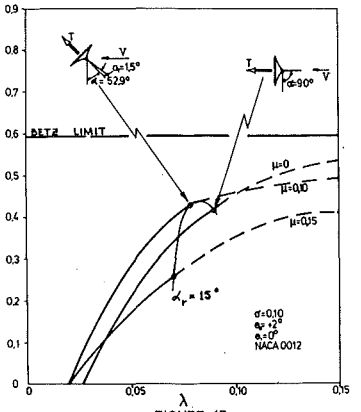

FIGURE 15

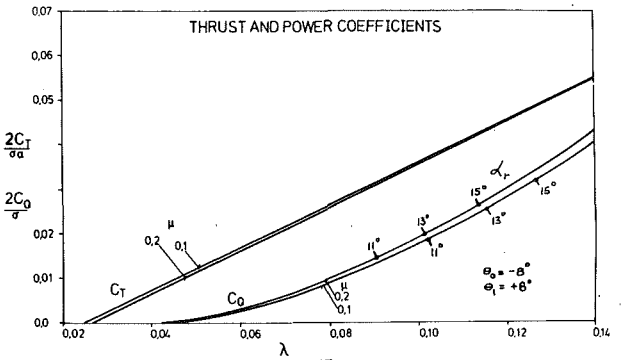

FIGURE 17

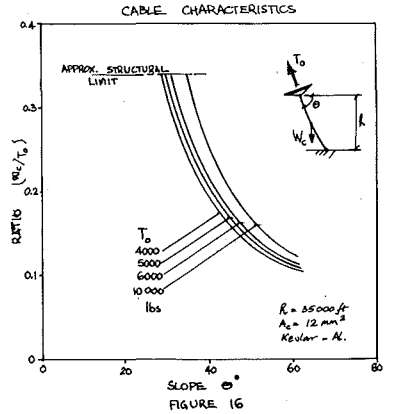

FIGURE 16

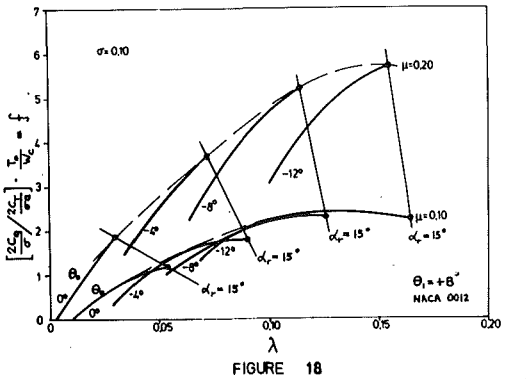

FIGURE 18

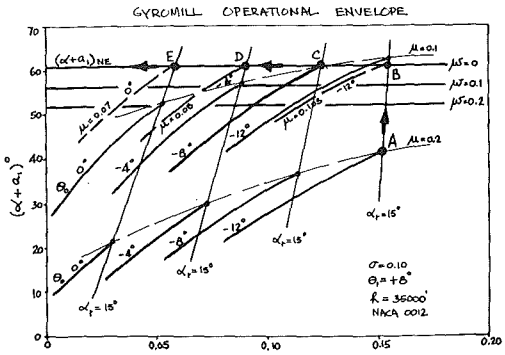

FIGURE 19

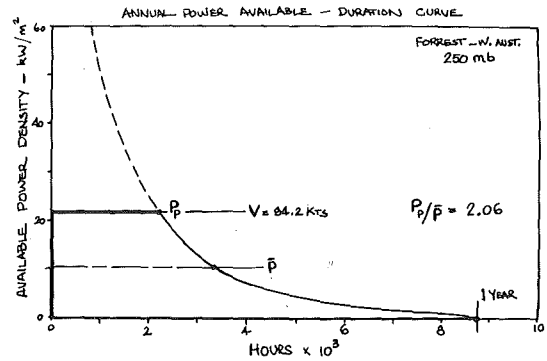

FIGURE 21

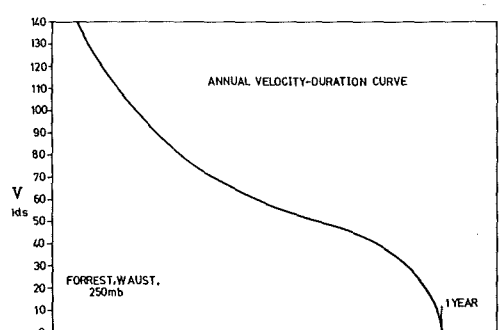

FIGURE 20

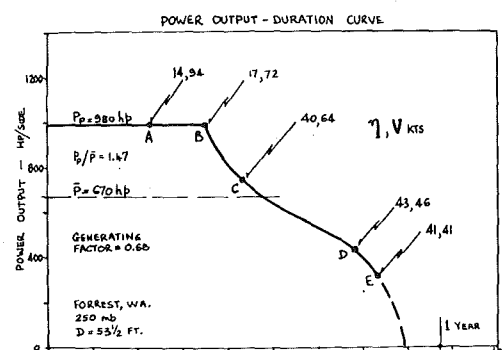

FIGURE 22